

Hidden and open heavy-flavor hadronic states

H. Garcilazo · A. Valcarce

Received: date / Accepted: date

Abstract We discuss the stability of hidden and open heavy-flavor hadronic states made of either two or three mesons. References are made in passing to studies regarding two and three-body systems containing baryons. We perform a comparative study analyzing the results in terms of quark and hadron degrees of freedom. Compact and molecular states are found to exist in very specific situations. We estimate the decay width for the different scenarios: weak decays for bound states by the strong interaction, and strong decays for hadronic resonances above a decay threshold. The experimental observation of narrow hadrons lying well above their lowest decay threshold is theoretically justified.

Keywords Few-body systems · Quark models · Exotic hadrons · Tetraquarks

1 Introduction

The hadron spectra above open-flavor thresholds has emerged as a key issue to understand QCD in the low-energy regime. The experimental hadron spectra below open-flavor thresholds follow closely a naive quark-antiquark ($q\bar{q}$) or three-quark (qqq) structure according to $SU(3)$ irreducible representations [1]. However, since 2003, several resonances reported by different experimental collaborations appeared close to a two-hadron threshold, presenting properties that makes a naive quark substructure unlikely. See, for example, Refs. [2, 3, 4, 5, 6, 7, 8] and references therein. Although this observation could be coincidental due to the large number of open-flavor thresholds in the energy region

H. Garcilazo
Escuela Superior de Física y Matemáticas,
Instituto Politécnico Nacional, Edificio 9, 07738 México D.F., Mexico
E-mail: humberto@esfm.ipn.mx

A. Valcarce
Departamento de Física Fundamental,
Universidad de Salamanca, E-37008 Salamanca, Spain
E-mail: valcarce@usal.es

where the new intriguing states have been reported, it could also point to a close relation between some particular thresholds and resonances contributing to the standard hadron spectroscopy.

The possible existence of hadrons with a quark content richer than $q\bar{q}$ or qqq states is nowadays a hot topic in hadron spectroscopy. Experimental discoveries have stimulated a flurry of theoretical studies dealing with multi-quark states and hadron-hadron resonances with a variety of different methodological approaches. It is important to note at the outset that conclusions drawn from hadron-hadron resonance analyses or a multi-quark constituent picture should be similar, provided that, in general, a coupled-channel hadron-hadron approach would be mandatory in order to reproduce the multi-quark constituent picture. To be more specific, let us note that multi-quark systems present a richer color structure than standard baryons or mesons. Whereas the color wave function for standard mesons and baryons is made of a single vector, for multi-quark states there are different vectors leading to a color singlet. For example, for four-quark states one can get a color singlet out of colorless singlet-singlet (11) or colored (88 , $\bar{3}3$, or $6\bar{6}$) components. Any colored component, better known as hidden-color vectors, can be expanded in terms of colorless singlet-singlet states [9,10] leading to a coupled-channel problem at hadronic level. Thus, an important question is whether one is in front of a colorless molecule or a compact state. Besides the color components, also the spatial distribution of the internal quark clusters is of great help to discriminate between the two structures [10].

Recently, the widely tackled sector of exotic states with two units of flavor, $QQ\bar{q}\bar{q}$, has been revitalized while their non-exotic partners, $Qq\bar{Q}\bar{q}$, have been much discussed in the context of the XYZ mesons [2,3,4,5,6,7,8]. In this contribution, we discuss the stability patterns of hidden and open heavy-flavor hadronic states made of two mesons, M_1M_2 and $M_1\bar{M}_2$ [11], and three mesons, $M_1M_2M_3$ [12]. References are made in passing to studies regarding two and three-body systems containing baryons [13,14,15,16]. We infer over-riding trends which are intended to reflect overall properties of the systems under study beyond peculiarities of a particular model. Thus, we will try to link results obtained using quark degrees of freedom with those derived in hadronic approaches using the common-sense rule of taking the same pairwise interaction. At present, this connection is a missing link in studies of low-energy hadron structure, and should be dealt with vigorously from the outset. This work could be a useful contribution to allow preliminary conclusions to be drawn. Finally, we will also present general results for the decay width of bound states by the strong interaction and hadronic resonances above a decay threshold [17,18,19].

2 General rationale based on symmetry breaking

The analogy between the stability of few-charge systems and multi-quarks in additive spin-independent potentials provides guidance on how to identify the

favorable multi-quark configurations that can lodge hadronic resonances and/or bound states. There are, however, some differences, not so much due to the radial shape of the potential, but mainly due to the color algebra replacing the simpler algebra of electric charges. The internal dynamics of multi-quark states is largely unknown and thus relies on some extrapolation from models that correctly accounts for the properties of ordinary mesons and baryons. The simplest and most widely used option consists of two-body potentials with simple color dependence, including both a spin-independent (chromoelectric) and a spin-dependent (chromomagnetic) component. We shall adopt here the so-called AL1 model by Semay and Silvestre-Brac [20]. It includes a standard Coulomb-plus-linear central potential, supplemented by a smeared version of the chromomagnetic interaction,

$$V(r) = -\frac{3}{16} \tilde{\lambda}_i \tilde{\lambda}_j \left[\lambda r - \frac{\kappa}{r} - A + \frac{V_{SS}(r)}{m_i m_j} \boldsymbol{\sigma}_i \cdot \boldsymbol{\sigma}_j \right],$$

$$V_{SS}(r) = \frac{2\pi\kappa'}{3\pi^{3/2}r_0^3} \exp\left(-\frac{r^2}{r_0^2}\right), \quad r_0 = A \left(\frac{2m_i m_j}{m_i + m_j}\right)^{-B}, \quad (1)$$

where $\lambda = 0.1653 \text{ GeV}^2$, $A = 0.8321 \text{ GeV}$, $\kappa = 0.5069$, $\kappa' = 1.8609$, $A = 1.6553 \text{ GeV}^{B-1}$, $B = 0.2204$, $m_u = m_d = 0.315 \text{ GeV}$, $m_s = 0.577 \text{ GeV}$, $m_c = 1.836 \text{ GeV}$ and $m_b = 5.227 \text{ GeV}$. Here, $\tilde{\lambda}_i \tilde{\lambda}_j$ is a color factor, suitably modified for the quark-antiquark pairs. The smearing parameter of the spin-spin term is adapted to the masses involved in the quark-quark or quark-antiquark pairs. The parameters of the AL1 potential are constrained in a simultaneous fit of 36 well-established mesons and 53 baryons, with a remarkable agreement with data, see Table 2 of Ref. [20].

To compute the ground-state of a $q\bar{q}$ meson or a qqq baryon in a constituent model, a crude variational approximation is often sufficient. For systems with a larger number of constituents the situation is drastically different. For example, for a tetraquark close to its threshold, one has to estimate precisely $q_1 q_2 \bar{q}_3 \bar{q}_4$ and its thresholds, to see whether there is a bound state. Moreover, the $q_1 q_2 \bar{q}_3 \bar{q}_4$ wave function has a $(q_1 \bar{q}_3)(q_2 \bar{q}_4)$ component and a $(q_1 \bar{q}_4)(q_2 \bar{q}_3)$ one, corresponding to its *molecular* part, perhaps a $(q_1 q_2)(\bar{q}_3 \bar{q}_4)$ *diquark-antidiquark* component, and a *collective* component that prevails in the event of deep binding.

Given that the chromomagnetic forces vanish in the limit of very heavy quarks, see Eq. (1), it is instructive to consider the case of a purely chromoelectric interaction to guide the search for optimal configurations to host hadronic resonances. Under these conditions, firm theoretical conclusions can be obtained. In quantum mechanics, it is well-known that breaking a symmetry lowers the ground-state energy¹. But in a few-body system, the breaking of symmetry often benefits more to the threshold than to the collective configuration and thus spoils the binding. From these results, one can analyze

¹ For instance, going from $H_0 = p^2 + x^2$ to $H_0 + \lambda x$, lowers the ground-state energy from $E_0 = 1$ to $E_0 - \lambda^2/4$, and more generally, breaking parity in $H = H_{\text{even}} + H_{\text{odd}}$ gives $E < E_{\text{even}}$.

the effect of symmetry breaking in systems of four-charged particles. Let us first consider the hydrogen molecule, $M^+M^+m^-m^-$. The Hamiltonian for this system reads,

$$H = \frac{\mathbf{p}_1^2}{2M} + \frac{\mathbf{p}_2^2}{2M} + \frac{\mathbf{p}_3^2}{2m} + \frac{\mathbf{p}_4^2}{2m} + V = H_0 + H_1$$

$$= \left[\sum_i \frac{\mathbf{p}_i^2}{2\mu} + V \right] + \left(\frac{1}{4M} - \frac{1}{4m} \right) (\mathbf{p}_1^2 + \mathbf{p}_2^2 - \mathbf{p}_3^2 - \mathbf{p}_4^2), \quad (2)$$

where $2\mu^{-1} = M^{-1} + m^{-1}$. The C -parity breaking term, H_1 , lowers the ground-state energy of H with respect to the C -parity even part, H_0 , which is simply a rescaled version of the Hamiltonian of the positronium molecule. Since H_0 and H have the same threshold, and since the positronium molecule is stable, the hydrogen molecule is even more stable, and stability improves when M/m increases. Clearly, the Coulomb character of V hardly matters in this reasoning. The key property is that the potential does not change when the masses are modified, a property named *flavor independence* in QCD.

One can use the same reasoning to study the stability of four-charged particles when C -parity is preserved but particle symmetry is broken, in other words the $M^+m^+M^-m^-$ configuration. The Hamiltonian is given by,

$$H = \frac{\mathbf{p}_1^2}{2M} + \frac{\mathbf{p}_2^2}{2m} + \frac{\mathbf{p}_3^2}{2M} + \frac{\mathbf{p}_4^2}{2m} + V = H_0 + H_1$$

$$= \left[\sum_i \frac{\mathbf{p}_i^2}{2\mu} + V \right] + \left(\frac{1}{4M} - \frac{1}{4m} \right) (\mathbf{p}_1^2 + \mathbf{p}_3^2 - \mathbf{p}_2^2 - \mathbf{p}_4^2). \quad (3)$$

On the basis of the arguments made above it is right to conclude that the ground-state of H gains binding with respect to the threshold $(M^+m^-) - (M^-m^+)$ that it shares with H_0 . However, there is another threshold that lies lower, $(M^+M^-) - (m^+m^-)$. This threshold gains more from the symmetry breaking than the four-body molecule, and, indeed, it is found that the molecule becomes unstable for $M/m \gtrsim 2.2$. In other words, a protonium atom cannot polarize enough a positronium atom and stick to it. It remains that the hydrogen-antihydrogen system could form a kind of metastable molecule below the atom-antiatom threshold [11,18].

In a semirelativistic framework the decomposition of H into a symmetric and an antisymmetric part under C -parity still holds, and the antisymmetric part lowers the ground state energy. However, H has not the same threshold as its symmetric part and one should study what wins, the asymmetry in the 4-body Hamiltonian or the one in the 2-body Hamiltonian [21].

Table 1 Properties of the $QQ\bar{q}\bar{q}$ ground state as a function of the mass of the heavy quark M_Q for the AL1 model [20]. Energies and masses are in MeV and distances in fm.

M_Q	Th	ΔE	$P[[\bar{3}\bar{3}]]$	$P[[\bar{6}\bar{6}]]$	P_{MM^*}	$P_{M^*M^*}$	\bar{x}	\bar{y}	\bar{z}
5227	10644	-151	0.967	0.033	0.561	0.439	0.334	0.784	0.544
4549	9290	-126	0.955	0.045	0.597	0.403	0.362	0.791	0.544
3871	7936	-100	0.930	0.070	0.646	0.354	0.411	0.806	0.541
3193	6582	-71	0.885	0.115	0.730	0.270	0.475	0.833	0.536
2515	5230	-41	0.778	0.222	0.795	0.205	0.621	0.919	0.523
1836	3878	-13	0.579	0.421	0.880	0.120	0.966	1.181	0.499
1158	2534	> 0	0.333	0.667	1.000	0.000	$\gg 1$	$\gg 1$	0.470

3 Two-meson states

3.1 Two-meson compact states: $QQ\bar{q}\bar{q} \equiv M_1M_2$

The arguments set out above after Eq. (2), can be directly translated to four-quark systems: the $QQ\bar{q}\bar{q}$ configuration becomes more and more bound when the mass ratio M/m increases. This has been established in the pioneering work of Ref. [22], and discussed and confirmed in further studies [23]². A remaining problem would be to understand why the positronium molecule lies slightly below its dissociation threshold, while a chromoelectric model associated with the color additive rule does not bind (at least according to most computations [23]). This is due to a larger disorder in the color coefficients than in the electrostatic strength factors entering the Coulomb potential [11]. Thus, multiquarks are penalized by the non-Abelian character of the color algebra, and its stability cannot rely on the asymmetries of the potential energy. It should use other asymmetries, in particular through the masses entering the kinetic energy, chromomagnetic effects generating mixing of $\bar{3}\bar{3}$ and $\bar{6}\bar{6}$ or the coupling to decay channels, etc.

We present in Table 1 the results for the ground state of a $QQ\bar{q}\bar{q}$ system with the AL1 potential [20], an isoscalar $J^P = 1^+$ state, as a function of the mass of the heavy quark M_Q [19]. For each value of M_Q we have evaluated the lowest strong-decay threshold, $Th = M_1 + M_2$, and the corresponding binding energy $B = -\Delta E$. The binding energy increases with increasing M_Q/m_q (m_q is kept constant). Close to $\Delta E = 0$ the system behaves like a simple meson-meson molecule, with a large probability in a single meson-meson component, the pseudoscalar-vector channel MM^* . However, when M_Q/m_q increases the probability of the $\bar{6}\bar{6}$ color component diminishes (it tends to zero for $M_Q \rightarrow \infty$). Therefore, heavy-light compact bound states would be almost a pure $\bar{3}\bar{3}$ color state and not a single colorless meson-meson molecule,

² It is worth to note that Ref. [13] derived the same conclusion for a three-body system of particles with masses $MM\mu$, with $M > \mu$. For non-interacting heavy-particles and an slightly attractive mass independent interaction between the light and heavy particles, the binding energy of the three-body system increases rapidly when M/μ augments, see Fig. 3 of Ref. [13].

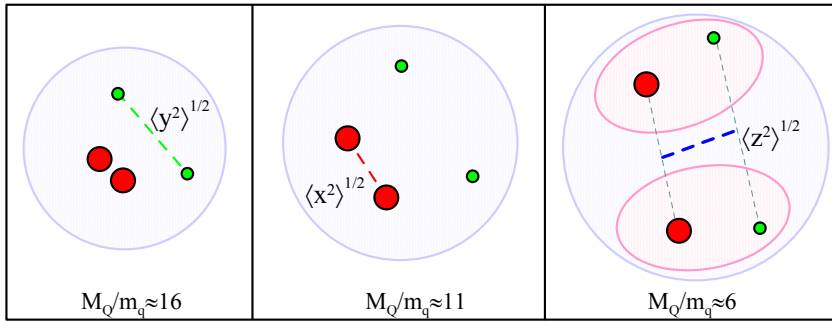


Fig. 1 Schematic representation of the internal structure of the $QQ\bar{q}\bar{q}$ ground state as the heavy-quark mass decreases and, accordingly, the binding energy.

11. Such compact states with internal colored components can be expanded in terms of physical meson-meson channels [9, 10], in this case pseudoscalar-vector MM^* and vector-vector M^*M^* components. Thus, $QQ\bar{q}\bar{q}$ states in the limit of large binding, i.e., M_Q/m_q large, can also be studied as a coupled-channel problem of physical meson-meson states leading to the same results [24, 25, 26]. Note however that the interaction between the clusters should be derived from the basic interactions between the constituents, which must be submitted to antisymmetrization [24]. Thus, a narrow spatial distribution would be also obtained [10].

The results in Table 1 show how when the binding increases, i.e. M_Q/m_q augments, the average distance between the two heavy quarks, $\bar{x} = \langle x^2 \rangle^{1/2}$, diminishes rapidly, while that of the two light quarks, $\bar{y} = \langle y^2 \rangle^{1/2}$, although diminishing, remains larger. The heavy-to-light quark distance, $\bar{z} = \langle z^2 \rangle^{1/2}$, stays almost constant for any value of M_Q/m_q . Thus, in the heavy-quark limit, the lowest lying tetraquark configuration resembles the Helium atom [27, 28, 29], a factorized system with separate dynamics for the compact color $\bar{3}$ QQ kernel and for the light quarks bound to the stationary color 3 state, to construct a $QQ\bar{q}\bar{q}$ color singlet. These results present a sharp picture of how the internal structure of the $QQ\bar{q}\bar{q}$ ground state changes according to the ratio M_Q/m_q , in other words, from a deeply bound compact state to a close-to-threshold meson-meson molecule, see Fig. 1.

A similar situation appears in the case of non-identical heavy-flavor mesons, or conversely systems of the type $QQ'\bar{q}\bar{q}$ [30]. Due to the existence of two distinguishable heavy quarks, there appears a strong-interaction stable $J^P = 0^+$ state below the 1^+ state discussed above for identical heavy quarks. The larger number of basis vectors contributing to a particular set of quantum numbers, some of which are forbidden in a system with identical heavy flavors, is relevant to understand how $QQ'\bar{q}\bar{q}$ bound states are formed.

Let us analyze how the dynamics of thresholds, see Fig. 2, helps to understand the results obtained for the $QQ'\bar{q}\bar{q}$ system. For this purpose we focus on the isoscalar $J^P = 1^+$ bound state, that exists both with identical (bb and

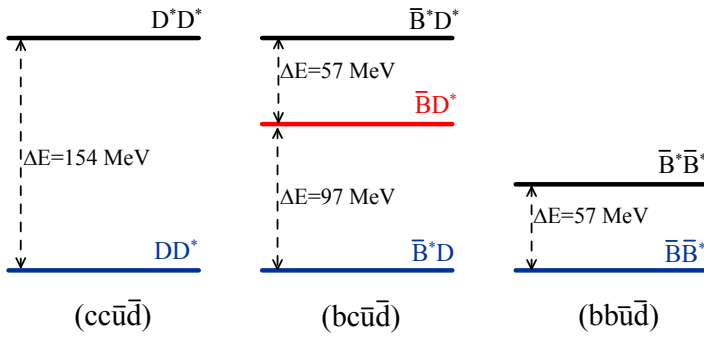


Fig. 2 Two-meson thresholds for the isoscalar $J^P = 1^+$ $cc\bar{u}\bar{d}$, $bc\bar{u}\bar{d}$, and $bb\bar{u}\bar{d}$ states.

cc) and non-identical (bc) heavy flavors. The chromomagnetic interaction, suppressed by M_Q as seen in Eq. (1), generates larger matrix elements in the charm than in the bottom sector between color-spin vectors of the pseudoscalar-vector and vector-vector two-meson components. However, as the mass difference between the two-meson components increases from 57 MeV in the bottom sector to 154 MeV in the charm one³, the coupling effect is weakened [31]. Since the single channel problem of DD^* or $\bar{B}\bar{B}^*$ mesons does not present bound states [10, 24], the weaker chromomagnetic coupling between DD^* and D^*D^* than between $\bar{B}\bar{B}^*$ and $\bar{B}^*\bar{B}^*$, leads to a reduction of the binding energy from 151 MeV in the bottom sector to 13 MeV in the charm one, see Table 1.

If we now consider the isoscalar $bc\bar{u}\bar{d}$ $J^P = 1^+$ state, the mass difference between \bar{B}^*D and \bar{B}^*D^* is the same as in the charm case, but the chromomagnetic interaction involving the bottom quark is weakened by a factor $m_b/m_c \sim 3$. Thus, a smaller binding energy than in the charm sector would be expected. However, the results exhibit a different trend, with a larger binding energy of 23 MeV [30]. What it is different about the $bc\bar{q}\bar{q}$ system is that it contains distinguishable heavy quarks and thus a new pseudoscalar-vector two-meson component (note that $\bar{M}_1M_2^*$ and $\bar{M}_1^*M_2$ have now a different mass) contributes to the $J^P = 1^+$ state. Besides, this new two-meson component, the $\bar{B}D^*$, is in between \bar{B}^*D and \bar{B}^*D^* , see Fig. 2. Interestingly enough, although the \bar{B}^*D and $\bar{B}D^*$ states are not directly coupled, nevertheless, they become indirectly coupled through the higher \bar{B}^*D^* state, i.e. $\bar{B}^*D \leftrightarrow \bar{B}^*D^* \leftrightarrow \bar{B}D^*$. Being the mass difference between \bar{B}^*D and $\bar{B}D^*$ smaller than between DD^* and D^*D^* the mixing is reinforced as compared to the charm case, leading to a binding energy larger than in the charm sector. The dynamics of thresholds to enhance or diminish coupled-channel effects has been illustrated at length in the literature [15, 32, 33, 34, 35, 36, 31]. However, Ref. [30] reported the first example where the presence of an additional intermediate threshold induced by the non-identity of the heavy quarks helps increasing the binding.

³ Results obtained with the AL1 model [20].

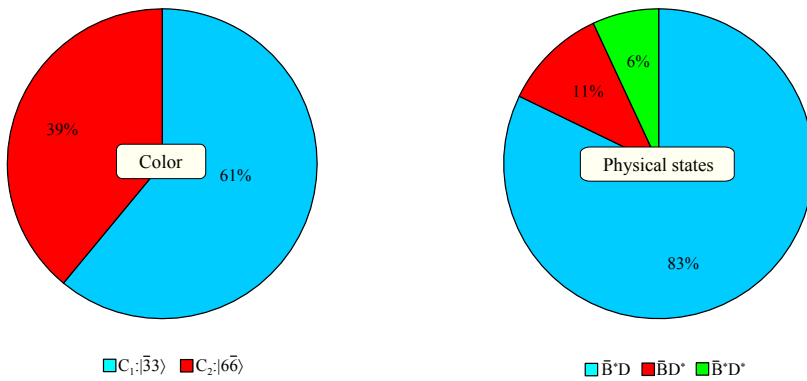


Fig. 3 Detailed structure of the isoscalar $bc\bar{u}\bar{d}$ $J^P = 1^+$ color wave function, showing the decomposition in terms of singlet-singlet color vectors, i.e., physical states [10].

Thus, there is an obvious link between studies based on quark degrees of freedom and those relying on hadronic models provided a coupled-channel approach is followed in the hadronic description. The equivalence can be analytically derived through the formalism developed in Ref. [10]. It allows to extract the probabilities of meson-meson physical channels out of a four-quark wave function expressed as a linear combination of color-spin-flavor-radial vectors. We show in Fig. 3 a summary of the color and meson-meson component probabilities for the isoscalar $J^P = 1^+$ $bc\bar{u}\bar{d}$ bound state. It is worth noting the 11% probability of the $\bar{B}D^*$ component, induced by the indirect coupling to the lowest \bar{B}^*D state through the highest \bar{B}^*D^* component. As has been recently discussed [23], these results present sound evidence about the importance of including a complete basis, i.e., not discarding any set of basis vectors a priori. Unless it is done that way, one is in front of approximations driving to unchecked results.

3.2 Two-meson molecular states: $Qq\bar{Q}\bar{q} \equiv M\bar{M}$

As discussed in Sect. 2 after Eq. (3), the presence of two thresholds for $Qq\bar{Q}\bar{q}$, one of them taking benefit from the breaking of the particle identity, makes a priori the stability of meson-antimeson states much more difficult. Hadrons with a $Qq\bar{Q}\bar{q}$ flavor content, could split either into $(Q\bar{q}) - (q\bar{Q})$ or $(Q\bar{Q}) - (q\bar{q})$ two-meson states [37]. For $Q = c$, the $(Q\bar{Q}) - (q\bar{q})$ and $(Q\bar{q}) - (q\bar{Q})$ thresholds are almost degenerate, while for $Q = b$ the $(Q\bar{Q}) - (q\bar{q})$ threshold is much lower than the $(Q\bar{q}) - (q\bar{Q})$ one as shown in Sect. 2. See also Fig. 4. The growth of the mass difference between the two thresholds when the mass of the heavy quark increases is linked to the flavor-independence of the chromoelectric interaction [39, 40, 41, 42]. Thus, the possibility of finding stable meson-antimeson molecules, $(Q\bar{q}) - (q\bar{Q})$, becomes more difficult when increasing the mass of the heavy flavor unless the two thresholds $(Q\bar{q}) - (q\bar{Q})$ and $(Q\bar{Q}) - (q\bar{q})$ would

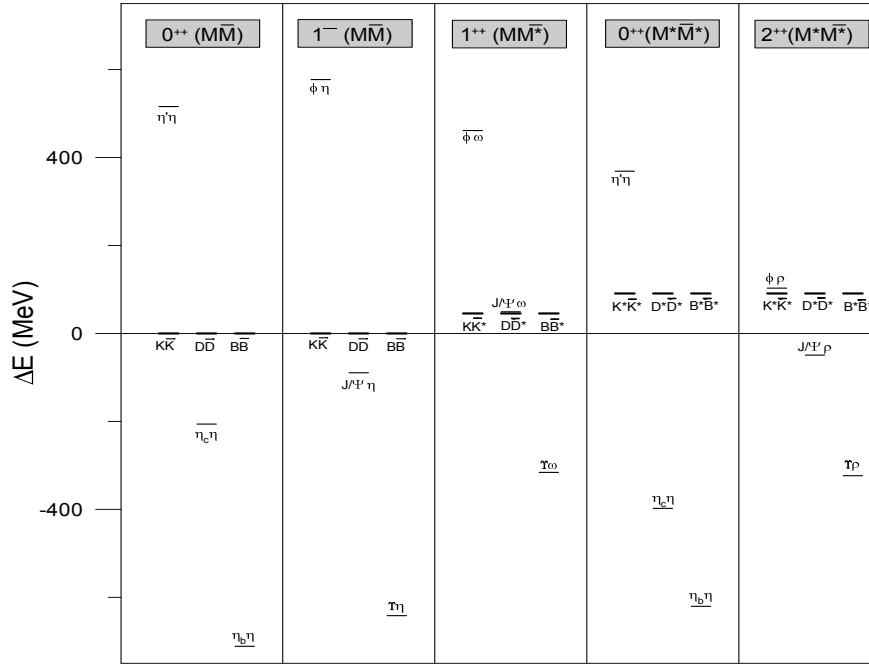


Fig. 4 Experimental masses [38] of the different two-meson $Qq\bar{Q}\bar{q}$ systems with $Q = s, c,$ or b , for several sets of quantum numbers, J^{PC} . The reference energy has been set to the $K\bar{K}$, $D\bar{D}$ and $B\bar{B}$ masses for the hidden strange, charm and bottom sectors, respectively.

be decoupled and thus a narrow quasibound state may arise [18], as will be discussed in Section 6.

The experimental scenario illustrated in Fig. 4 suggests different consequences for meson-antimeson molecules. First, the possible existence of stable molecules in the hidden-strange sector. If the $K\bar{K}$ interaction were attractive, this two-meson system may be stable because no any other threshold appears below. This was precisely the idea suggested by Weinstein and Isgur [43] as a plausible explanation of the proliferation of scalar mesons in the light sector. Second, the possibility of finding meson-meson molecules contributing to the charmonium spectrum due to the coupled-channel dynamics, as in the case of the $(I)J^{PC} = (0)1^{++}$ quantum numbers. In this case the isoscalar $(c\bar{q}) - (q\bar{c}) \equiv D\bar{D}^*$ and $(c\bar{c}) - (q\bar{q}) \equiv J/\psi \omega$ two-body channels are so close together⁴ that a slightly attractive interaction along with the cooperative effect of the almost degenerate two-body channels provides a plausible explanation of the $X(3872)$ [44, 45].

In spite of the widespread belief that the stability of a multiquark state is favored by increasing the mass of the heavy flavors, the structures studied in

⁴ Note that the vicinity of thresholds is a necessary though not sufficient condition for the existence of a resonance. See Ref. [25] for a thorough and critical analysis.

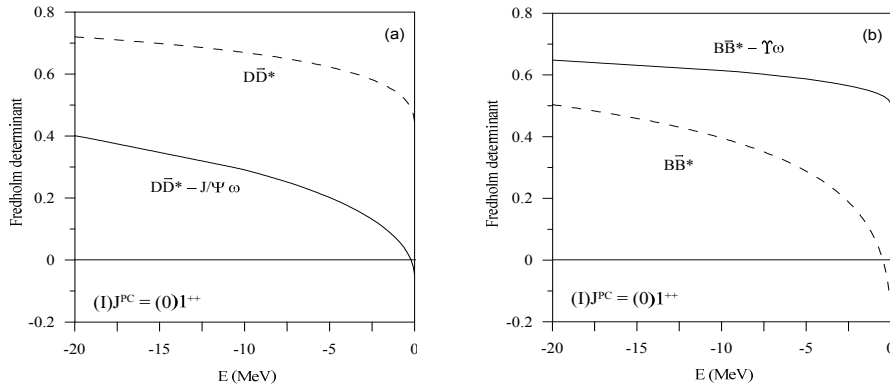


Fig. 5 (a) $(I)J^{PC} = (0)1^{++}$ $cq\bar{c}\bar{q}$ Fredholm determinant. The dashed line stands for a calculation considering only charmed mesons, $D\bar{D}^*$, whereas the solid line includes the coupling to the $J/\Psi \omega$ two-meson state. (b) Same as (a) for bottomonium.

this section send a clear warning that it is not always the case⁵. The reason is that the mass of one of the thresholds, $(Q\bar{Q}) - (q\bar{q})$, diminishes rapidly when the heavy quark mass increases. This simple reasoning, formulated in terms of coupled-channel arguments, is illustrated in Fig. 5. In Fig. 5(a) it can be seen how the $D\bar{D}^*$ interaction (dashed line) is not attractive enough to generate a bound state (the Fredholm determinant falls short of being negative [47]). The coupling to the $J/\Psi \omega$ channel (solid line) is responsible for having a bound state just below threshold. Note that this plausible explanation of the $X(3872)$ is strengthened by the subsequent experimental observation of the decay $X(3872) \rightarrow J/\Psi \omega$ [48]. When the mass of the heavy quark augments from charm to bottom, the $B\bar{B}^*$ interaction becomes more attractive, dashed line in Fig. 5(b). However, the coupling to the lower channel, $\Upsilon \omega$, would destroy the possibility of having a bound state, solid line in Fig. 5(b). Thus, based on constituent model arguments, one should not expect a twin of the $X(3872)$ in the bottom sector, as pointed out by hadronic models based on the traditional meson theory of the nuclear forces [49] or resorting to heavy quark symmetry arguments [50,51]. Note however, that if the $B\bar{B}^*$ and $\Upsilon \omega$ channels were decoupled, as it is suggested by the rescaling [52] of recent lattice QCD calculations of the interaction of the J/Ψ with nuclear matter [53], the arguments put forward by Ref. [18] on the basis of the results shown in Fig. 5(b) would justify that a narrow resonance might appear just below the $B\bar{B}^*$ threshold.

⁵ See, for example, Ref. [46] for a further demonstration of the instability of all-heavy tetraquarks $QQ\bar{Q}\bar{Q}$ with a rigorous treatment of the few-body problem.

Table 2 Different two-body channels (i, j) contributing to the $(I)J^P = (1/2)2^-$ $BB^*B^* - B^*B^*B^*$ system.

Interacting pair	(i, j)	Spectator
BB^*	(0, 1)	B^*
	(1, 1)	
B^*B^*	(0, 1)	B^*
	(1, 2)	
B^*B^*	(1, 2)	B

4 Three-meson bound states

The broad theoretical consensus [22, 23, 28, 54, 55, 56, 57, 58, 59, 60, 61] on the existence of an isoscalar doubly bottom tetraquark, T_{bb} ⁶, discussed in Sect. 3.1, opens the door to the possible existence of other bound states with a larger number of hadrons [12, 15, 62]. The answer is by no means trivial. Ref. [15] studied three-body systems containing D and \bar{B} mesons together with nucleons and Δ 's. It was shown that if the different two-body thresholds of a three-body system are far away, they conspire against the stability of the three-body system. Thus, in this section we review the stability of systems made of three B mesons.

We solve exactly the Faddeev equations for the three-meson bound state problem [12] using as input the two-body t -matrices of a constituent model [15]. We select those $(I)J^P$ three-body channels that contain the T_{bb} state and where two-body subsystems containing two B -mesons are not allowed, because the BB interaction does not show an attractive character. The three-body channel $(I)J^P = (1/2)2^-$ is the only one bringing together all these conditions to maximize the possible binding of the three-body system⁷. We indicate in Table 2 the two-body channels contributing to this state that we examine in the following, leading to a coupled-channel problem of pseudoscalar-vector and vector-vector two B -meson components.

The Lippmann-Schwinger equation for the bound-state three-body problem is

$$T = (V_1 + V_2 + V_3)G_0T, \quad (4)$$

where V_i is the potential between particles j and k and G_0 is the propagator of three free particles. The Faddeev decomposition of Eq. (4),

$$T = T_1 + T_2 + T_3, \quad (5)$$

leads to the set of coupled equations,

$$T_i = V_iG_0T. \quad (6)$$

⁶ The binding energy reported for the T_{bb} tetraquark ranges between 90 and 214 MeV.

⁷ Note that the three-body channels with $J = 0$ or 1 would couple to two B -meson subsystems where no attraction has been reported [22, 23, 28, 54, 55, 56, 57, 58, 59, 60, 61], whereas the $J = 3$ would not contain a two-body subsystem with $j = 1$, the quantum numbers of the T_{bb} tetraquark. The same reasoning excludes the $I = 3/2$ channels.

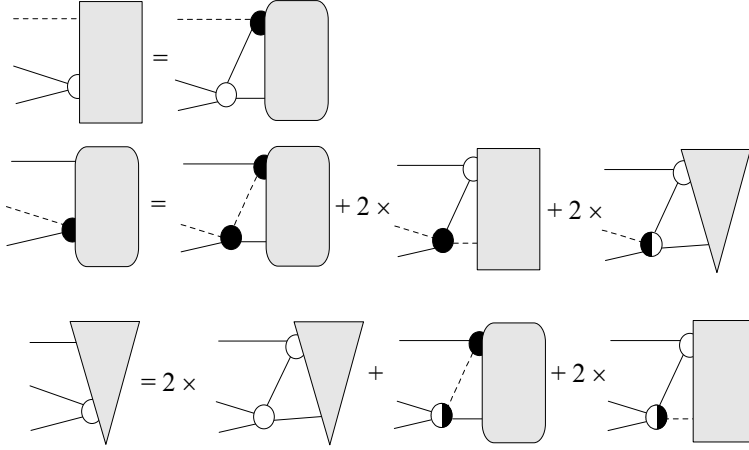


Fig. 6 Diagrammatic Faddeev equations for the three B -meson system.

The Faddeev decomposition guarantees the uniqueness of the solution [63, 64]. Eqs. (6) can be rewritten in the Faddeev form

$$T_i = t_i G_0 (T_j + T_k), \quad (7)$$

with

$$t_i = V_i + V_i G_0 t_i, \quad (8)$$

where t_i are the two-body t -matrices that already contain the coupling among all two-body channels contributing to a given three-body state. The two sets of equations (6) and (7) are completely equivalent for the bound-state problem. In the case of two three-body systems that are coupled together, like $BB^*B^* - B^*B^*B^*$, the amplitudes T_i become two-component vectors and the operators V_i , t_i , and G_0 become 2×2 matrices and lead to the equations depicted in Fig. 6. The solid lines represent the B^* mesons and the dashed lines the B meson. If in the second equation depicted in Fig. 6 one drops the last term in the r.h.s. then the first and second equations become the Faddeev equations of two identical bosons plus a third one that is different [15]. Similarly, if in the third equation depicted in Fig. 6 one drops the last two terms this equation becomes the Faddeev equation of a system of three identical bosons since in this case the three coupled Faddeev equations are identical [15]. The additional terms in Fig. 6 are, of course, those responsible for the coupling between the BB^*B^* and $B^*B^*B^*$ components.

We show in Fig. 7 the results of our calculation. The blue solid lines stand for the different three B -meson strong decay thresholds of the $BB^*B^* - B^*B^*B^*$ system with quantum numbers $(I)J^P = (1/2)2^-$, that we have denoted by T_{bbb} . These thresholds are $B^*B^*B^*$, BB^*B^* and $T_{bb}B^*$. The green dashed lines stand for the possible three B -meson electromagnetic decay thresholds, BBB^* and BBB with quantum number $(I)J^P = (1/2)1^-$

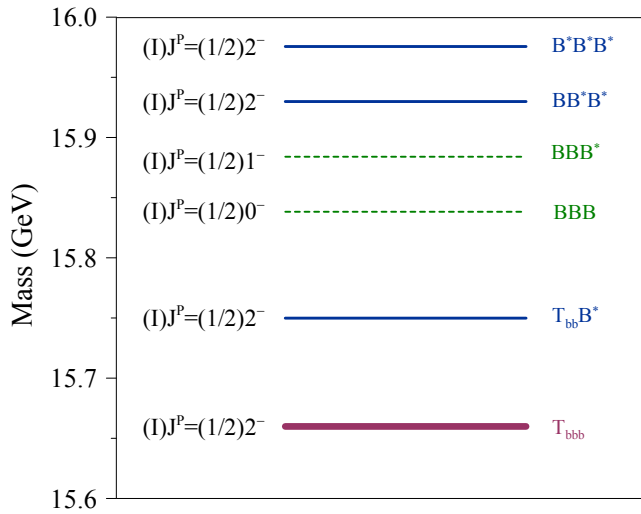


Fig. 7 Mass of the three-body $BB^*B^* - B^*B^*B^*$ bound-state $(I)J^P = (1/2)2^-$ T_{bbb} (purple thick line), compared to the different three B -meson strong (blue solid lines) and electromagnetic (green dashed lines) decay thresholds.

and $(I)J^P = (1/2)0^-$, respectively. Finally, the purple thick line indicates the energy of the T_{bbb} , that appears 90 MeV below the lowest threshold. The results shown in Fig. 7 correspond to the binding energy of the T_{bb} obtained in Ref. [55].

We have checked that the T_{bbb} remains stable for the whole range of binding energies of the T_{bb} reported in the literature, repeating the coupled-channel three-body calculation starting from the smallest binding of the order of 90 MeV obtained in Ref. [57]. The results are given in Table 3. It can be seen how the three-meson bound state T_{bbb} is comfortably stable. If the binding energy of the T_{bb} is reduced up to 50 MeV, the three-body system would have a binding of the order of 23 MeV that would already lie 19 MeV above the lowest BBB threshold, so that one does not expect any kind of Borromean binding. It is worth noting that many-body interactions inspired

Table 3 Binding energy, in MeV, of the T_{bbb} $(I)J^P = (1/2)2^-$ $BB^*B^* - B^*B^*B^*$ three-body system as a function of the binding energy, in MeV, of the T_{bb} tetraquark. The T_{bbb} binding energy is calculated with respect to the lowest strong decay threshold: $m_B + 2m_{B^*} - B(T_{bb})$.

$B(T_{bb})$	$B(T_{bbb})$
180	90
144	77
117	57
87	43

by the strong-coupling regime of QCD do not support stability of four-quark exotic states, see the solid line in Fig. 2 of Ref. [65] and, thus, they are not expected to play a relevant role for the T_{bbb} .

If the T_{bbb} would have appeared in between the two three-body thresholds, BB^*B^* and $B^*B^*B^*$, it could still be narrow. Ref. [17] has presented a plausible argument based on first-order perturbation theory explaining the small width of a three-body resonance in a coupled two-channel system lying close to the upper channel in spite of being open the lower one. This is a challenging result when the available phase space of the decay channel is quite large. Similar arguments could be handled for a comprehensive study of the properties of the LHCb pentaquarks [2,3,4,5,6,7,8,16]. However, this would require a thorough analysis within each particular model used to study these states.

5 Decay width of $QQ\bar{q}\bar{q}$ states

For a representative state below all possible strong-decay thresholds, for example the T_{bb} tetraquark discussed in Sect. 3.1, we have calculated its decay width due to all plausible semileptonic and nonleptonic decay modes [19]. Some of the corresponding processes are illustrated in Fig. 8. The hadronic decays are calculated within the factorization approximation [66]. The largest partial widths are found to be of the order of 10^{-15} to 10^{-14} GeV. For the semileptonic modes, the corresponding decays are of the type $\bar{B}^*D^*\ell^-\bar{\nu}_\ell$, where $\ell = e$ or μ . Due to the large phase space available in all cases, the differences among the widths into the three lepton families are very small.

For semileptonic decays with two mesons in the final state, the processes involving a $b \rightarrow c$ vertex are favored compared to those involving a $b \rightarrow u$ vertex, due to the larger CKM matrix element. In Table 4 we show the most favorable channels, the filter being a width larger than $10^9 \text{ s}^{-1} = 0.66 \times 10^{-15} \text{ GeV}$, for the semileptonic decays with two mesons and a light $\ell = e, \mu$ lepton in the final state. Though much smaller, we also give the widths for the corresponding channels with a final τ since they could be interesting in the context of studies of lepton-flavor universality violation. Besides, due to spin recoupling coefficients, the largest decay widths appear for vector mesons in the final state.

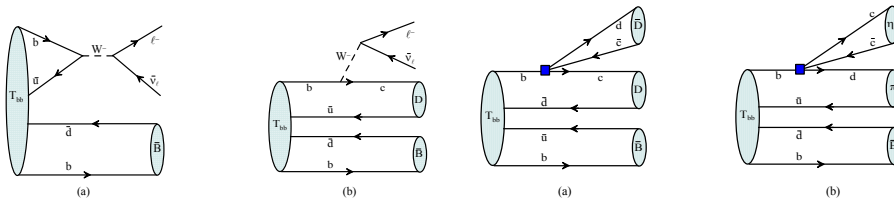


Fig. 8 Representative diagrams for semileptonic (left) and nonleptonic (right) decays of the T_{bb} tetraquark.

Table 4 Decay widths, in units of 10^{-15} GeV, of the leading semileptonic modes of T_{bb} .

Final state	Γ	Final state	Γ
$B^{*-} D^{*+} \ell^- \bar{\nu}_\ell$	9.02 ± 0.07	$B^{*-} D^{*+} \tau^- \bar{\nu}_\tau$	1.55 ± 0.01
$\bar{B}^{*0} D^{*0} \ell^- \bar{\nu}_\ell$		$\bar{B}^{*0} D^{*0} \tau^- \bar{\nu}_\tau$	
$B^{*-} D^+ \ell^- \bar{\nu}_\ell$	3.59 ± 0.03	$B^{*-} D^+ \tau^- \bar{\nu}_\tau$	0.727 ± 0.005
$\bar{B}^{*0} D^0 \ell^- \bar{\nu}_\ell$		$\bar{B}^{*0} D^0 \tau^- \bar{\nu}_\tau$	
$B^- D^{*+} \ell^- \bar{\nu}_\ell$	4.63 ± 0.05	$B^- D^{*+} \tau^- \bar{\nu}_\tau$	0.86 ± 0.007
$\bar{B}^0 D^{*0} \ell^- \bar{\nu}_\ell$		$\bar{B}^0 D^{*0} \tau^- \bar{\nu}_\tau$	
$B^- D^+ l^- \bar{\nu}_l$	1.92 ± 0.02	$B^- D^+ \tau^- \bar{\nu}_\tau$	0.409 ± 0.003
$\bar{B}^0 D^0 \ell^- \bar{\nu}_\ell$		$\bar{B}^0 D^0 \tau^- \bar{\nu}_\tau$	

For the nonleptonic decays, the largest widths are for the decays of the type $\bar{B}^* D^* D_s^*$. All of them contain a $b \rightarrow c$ vertex and a D_s^* meson in the final state. See Table 5. Once again vector mesons are favored in the final state. Processes with D_s or a light meson final state arising from vacuum have decay widths comparable to the corresponding semileptonic decay.

Finally, as it has been suggested the possible existence of an strong-stable isoscalar T_{bc} tetraquark with quantum numbers $J^P = 0^+$ [30,56], we evaluate the decay $T_{bb}(1^+) \rightarrow T_{bc}(0^+) \ell^- \nu_\ell$ which is 7.5×10^{-15} GeV. The semileptonic decay to the 0^+ T_{bc} tetraquark is relevant but it is not found to be dominant in clear disagreement with the result of Ref. [67], obtained using a QCD three-point sum rule approach.

We also estimated all plausible decay modes such as $\bar{B}^0 e^- \bar{\nu}_e$, or $B^{*-} D^+ \pi^-$, etc. The total width turns out to be about 87×10^{-15} GeV, which gives an upper bound for the lifetime of about 7.6 ps. This lifetime is one order of magnitude larger than the simplest guess-by-analogy estimation of 0.3 ps of Ref. [56]. It is important to note that a long lifetime for the T_{bb} tetraquark can ease its detection through the method of *displaced vertex* proposed in Ref. [68].

Table 5 Decay widths, in units of 10^{-15} GeV, of the leading nonleptonic modes of T_{bb} .

Final state	Γ	Final state	Γ
$B^{*-} D^{*+} D_s^-$	4.00 ± 0.06	$B^- D^{*+} D_s^{*-}$	3.15 ± 0.05
$\bar{B}^{*0} D^{*0} D_s^-$		$\bar{B}^0 D^{*0} D_s^{*-}$	
$B^{*-} D^{*+} D_s^{*-}$	6.50 ± 0.09	$B^- D^+ D_s^{*-}$	1.20 ± 0.02
$\bar{B}^{*0} D^{*0} D_s^{*-}$		$\bar{B}^0 D^0 D_s^{*-}$	
$B^{*-} D^+ D_s^-$	2.57 ± 0.04	$B^{*-} D^{*+} \rho^-$	3.57 ± 0.09
$\bar{B}^{*0} D^0 D_s^-$		$B^{*-} D^{*+} \pi^-$	1.28 ± 0.03
$B^{*-} D^+ D_s^{*-}$	2.32 ± 0.03	$B^{*-} D^+ \rho^-$	1.70 ± 0.04
$\bar{B}^{*0} D^0 D_s^{*-}$		$B^{*-} D^+ \pi^-$	0.70 ± 0.02
$B^- D^{*+} D_s^-$	2.78 ± 0.05	$B^- D^{*+} \rho^-$	2.01 ± 0.05
$\bar{B}^0 D^{*0} D_s^-$		$B^- D^{*+} \pi^-$	0.77 ± 0.03

6 Decay width of $Qq\bar{Q}\bar{q}$ states

We have finally addressed the study of the decay width for those cases where a resonance is produced between two thresholds, thanks to a coupling between two internal configurations within the resonance [18]. For this purpose, we have modeled the system as a coupled-channel problem obeying the non-relativistic Lippmann-Schwinger equation. Channel 1, the lowest in mass, consists of two particles with masses m_1 and m_2 , and channel 2, the upper in mass, is made of two particles with masses m_3 and m_4 . The Lippmann-Schwinger equation is written as,

$$t^{ij}(p, p'; E) = V^{ij}(p, p') + \sum_{k=1,2} \int_0^\infty p''^2 dp'' \frac{V^{ik}(p, p'') t^{kj}(p'', p'; E)}{E - \Delta M \delta_{2,k} - \frac{p''^2}{2\mu_k} + i\epsilon}, \quad (9)$$

where $i, j = 1, 2$, $\mu_1 = m_1 m_2 / (m_1 + m_2)$ and $\mu_2 = m_3 m_4 / (m_3 + m_4)$ are the reduced masses of channels 1 and 2, and $\Delta M = m_3 + m_4 - m_1 - m_2$ with $m_3 + m_4 > m_1 + m_2$. The interaction kernels in momentum space are given by,

$$V^{ij}(p, p') = \frac{2}{\pi} \int_0^\infty r^2 dr j_0(pr) V^{ij}(r) j_0(p'r), \quad (10)$$

where the two-body potentials, which are the inputs of the modeling, consist of an attractive and a repulsive Yukawa term, i.e.,

$$V^{ij}(r) = -A \frac{e^{-\mu_A r}}{r} + B \frac{e^{-\mu_B r}}{r}. \quad (11)$$

We have considered scenarios where a resonance exists at an energy $E = E_R$, such that the phase shift $\delta(E_R) = 90^\circ$, for energies between the thresholds of channels 1 and 2, i.e., $0 < E_R < \Delta M$. The mass of the resonance is given by $M_R = E_R + m_1 + m_2$, and its width is calculated using the Breit-Wigner formula as [69, 70, 71],

$$\Gamma(E) = \lim_{E \rightarrow E_R} \frac{2(E_R - E)}{\cotg[\delta(E)]}. \quad (12)$$

By varying the parameters in Table 6, one can control the existence of a bound state or a resonance and its relative position with respect to the thresholds. We choose as starting point the set of parameters given in Table 6. They are adjusted such that in a single-channel calculation, the upper channel (channel 2) has a bound state just at threshold, while in a coupled-channel calculation, the full system has a bound state just at the lower threshold. If one increases the magnitude of the repulsive term in the lower channel, $B(1 \leftrightarrow 1)$ in Table 6, the bound state of the coupled-channel system moves up and actually becomes a resonance into the continuum. One can study the behavior of its width when its mass evolves from the lower threshold, channel 1, to the upper one, channel 2. The result is shown in Fig. 9.

The width of the resonance starts increasing quickly when getting away from the lower threshold, but at about a third of the way towards the upper channel, the width starts to decrease although the phase space for the decay to channel 1, where the resonance is observed, still increases⁸. It is important to note that the strength of the coupling between the two thresholds has not been modified. When the resonance approaches the upper threshold, it becomes narrow and seemingly ignores the existence of the lower threshold. The wave function of the (m_3, m_4) bound state of vanishing energy has, indeed, little overlap with the (m_1, m_2) configuration. The same trend is obtained for different strengths of the coupling interaction in Table 6 or varying the mass difference between the two thresholds [18]. Hence, in this region, the dynamics is dominated by the attraction in the upper channel and the second channel is mainly a tool for the detection. This mechanism is somewhat related to the 'synchronization of resonances' proposed by D. Bugg [72].

The mechanism we have discussed above could help to understand the narrow width of several of the hidden heavy-flavor resonances with a large phase space in a decay channel that have been recently reported in both the meson and baryon sectors, whose hypothetical internal structure would allow them to split into different subsystems [2, 3, 4, 5, 6, 7, 8]. This would apply, for example, to the $B\bar{B}^*$ state of Fig. 5(b). The situation resembles a Feshbach resonance, where the open channel is represented by the $\Upsilon\omega$ state that would get trapped in a molecular state supported by the closed channel potential $B\bar{B}^*$ [73, 74]. An unexpected behavior of the width of the resonance may be indicating an important contribution of coupled-channel dynamics and the knowledge of the decay width in a particular channel would hint to the upper threshold contributing to the formation of the resonance. This has been illustrated in Fig. 10, where we have calculated the width of the resonance for a fixed value of its mass with respect to the lower threshold, $\Delta E_{Th} = M_R - m_1 - m_2 = 6.5$ MeV, but increasing the distance with respect to the upper threshold, $\Delta E'_{Th} = m_3 + m_4 - M_R$. For this purpose, we have diminished the mass of the lower channel in steps of 5 MeV, thus increasing the distance between thresholds, $m_3 + m_4 - m_1 - m_2$, and we have increased $A(1 \leftrightarrow 1)$ in Table 6 in such a way that $\Delta E_{Th} = M_R - m_1 - m_2 = 6.5$ MeV remains constant. The result

⁸ Although the Breit-Wigner formula is not very accurate close to threshold; however, we have explicitly checked by analytic continuation of the S-matrix on the second Riemann sheet that at low energy the width follows the expected $\Gamma \sim E^{1/2}$ behavior, the one shown by Fig. 9.

Table 6 Parameters of the interaction as given in Eq. (11). A and B are in MeV fm, while μ_A and μ_B are in fm^{-1} . $m_1 = m_2 = 1115.7 \text{ MeV}/c^2$, $m_3 = 938.8 \text{ MeV}/c^2$, and $m_4 = 1318.2 \text{ MeV}/c^2$.

Channel	A	μ_A	B	μ_B
$1 \leftrightarrow 1$	100	2.68	667	5.81
$2 \leftrightarrow 2$	680	4.56	642	6.73
$1 \leftrightarrow 2$	200	1.77	195	3.33

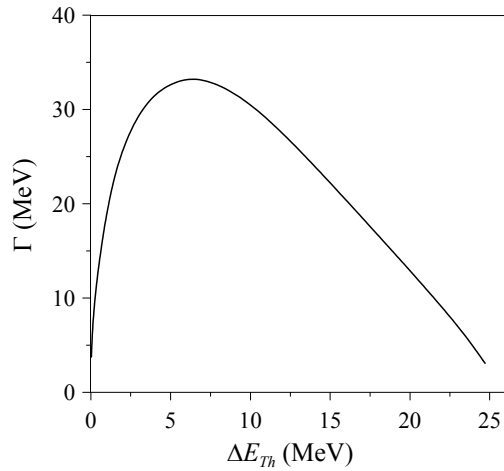


Fig. 9 Width of the resonance, Γ , as a function of the energy difference between its mass and the mass of the lower threshold generating the state, $\Delta E_{Th} = M_R - m_1 - m_2$. The upper channel is 25.6 MeV above the lower one.

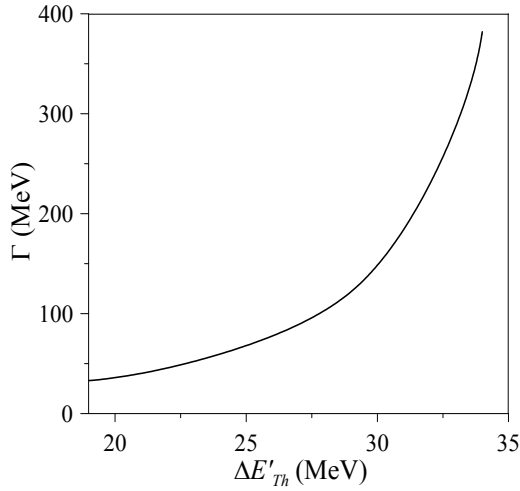


Fig. 10 Width of the resonance, Γ , as a function of the energy difference between its mass and the mass of the upper threshold generating the state, $\Delta E'_{Th} = m_3 + m_4 - M_R$, for a fixed energy with respect to the lower threshold, $\Delta E_{Th} = M_R - m_1 - m_2 = 6.5$ MeV.

is striking, being the phase space fixed for the detection channel, the width increases when the upper threshold moves away. Thus the width provides also with basic information about the coupled channels that may contribute to the formation of a resonance. The observation of a small width in a low-lying channel hints to a dominant contribution of some upper channel to the formation of the resonance. Thus, although the exact shape of the dependence of

the width on its position with respect to the detection channel would depend on the specific dynamics of the coupled-channel system, the gross features reflected here might be a relevant and basic hint to explore the nature of some of the exotic states.

Acknowledgements The authors are deeply indebted to their long-term collaborators T. F. Caramés, E. Hernández, J. -M. Richard and J. Vijande that have participated in some of the issues reviewed in this work. This work has been partially funded by COFAA-IPN (México) and by Ministerio de Economía, Industria y Competitividad and EU FEDER under Contracts No. FPA2016-77177 and RED2018-102572-T.

References

1. M. Gell-Mann, Phys. Lett. **8**, 214 (1964).
2. H. -X. Chen, W. Chen, X. Liu, S. -L. Zhu, Phys. Rep. **639**, 1 (2016).
3. R. A. Briceño *et al.*, Chin. Phys. C **40**, 042001 (2016).
4. J. -M. Richard, Few-Body Syst. **57**, 1185 (2016).
5. R. F. Lebed, R. E. Mitchell, E. S. Swanson, Prog. Part. Nucl. Phys. **93**, 143 (2017).
6. A. Ali, J. S. Lange, S. Stone, Prog. Part. Nucl. Phys. **97**, 123 (2017).
7. A. Esposito, A. Pilloni, A. D. Polosa, Phys. Rep. **668**, 1 (2017).
8. Y. -R. Liu, H. -X. Chen, W. Chen, X. Liu, S. -L. Zhu, Prog. Part. Nucl. Phys. **107**, 237 (2019).
9. M. Harvey, Nucl. Phys. **352**, 301 (1981).
10. J. Vijande, A. Valcarce, Phys. Rev. C **80**, 035204 (2009).
11. A. Valcarce, J. Vijande, J.- M. Richard, H. Garcilazo, Few-Body Syst. **59**, 9 (2018).
12. H. Garcilazo, A. Valcarce, Phys. Lett. B **784**, 169 (2018).
13. H. Garcilazo, Phys. Rev. C **30**, 765 (1984).
14. T. F. Caramés, A. Valcarce, Phys. Rev. D **85**, 094017 (2012).
15. H. Garcilazo, A. Valcarce, T. F. Caramés, Phys. Rev. D **96**, 074009 (2017).
16. J. -M. Richard, A. Valcarce, J. Vijande, Phys. Lett. B **774**, 710 (2017).
17. H. Garcilazo, A. Valcarce, Phys. Lett. B **772**, 394 (2017).
18. H. Garcilazo, A. Valcarce, Eur. Phys. J. C **78**, 259 (2018).
19. E. Hernández, J. Vijande, A. Valcarce, J. -M. Richard, Phys. Lett. B **800**, 135073 (2020).
20. C. Semay, B. Silvestre-Brac, Z. Phys. C **61**, 271 (1994).
21. J. -M. Richard, private communication and work in progress.
22. J. -P. Ader, J. -M. Richard, P. Taxil, Phys. Rev. D **25**, 2370 (1982).
23. J. -M. Richard, A. Valcarce, J. Vijande, Phys. Rev. C **97**, 035211 (2018).
24. T. F. Caramés, A. Valcarce, J. Vijande, Phys. Lett. B **699**, 291 (2011).
25. J. Vijande, A. Valcarce, Phys. Lett. B **736**, 325 (2014).
26. Y. Ikeda, B. Charron, S. Aoki, T. Doi, T. Hatsuda, T. Inoue, N. Ishii, K. Murano, H. Nemura, K. Sasaki, Phys. Lett. B **729**, 85 (2014).
27. H. J. Lipkin, Phys. Lett. B **172**, 242 (1986).
28. E. J. Eichten, C. Quigg, Phys. Rev. Lett. **119**, 202002 (2017).
29. C. Quigg, in *53rd Rencontres de Moriond QCD High Energy Interactions Conference*, La Thuile, Italy (2018), arXiv:1804.04929 [hep-ph].
30. T. F. Caramés, J. Vijande, A. Valcarce, Phys. Rev. D **99**, 014006 (2019).
31. T. F. Caramés, A. Valcarce, Phys. Lett. B **758**, 244 (2016).
32. M. F. M. Lutz, E. E. Kolomeitsev, Nucl. Phys. A **755**, 29c (2005).
33. H. Garcilazo, T. Fernández-Caramés, A. Valcarce, Phys. Rev. C **75**, 034002 (2007).
34. H. Garcilazo, A. Valcarce, T. Fernández-Caramés, Phys. Rev. C **76**, 034001 (2007).
35. H. Garcilazo, A. Valcarce, T. F. Caramés, Phys. Rev. C **92**, 024006 (2015).
36. T. Barnes, F. E. Close, E. S. Swanson, Phys. Rev. D **91**, 014004 (2015).
37. T. F. Caramés, A. Valcarce, J. Vijande, Phys. Lett. B **709**, 358 (2012).
38. M. Tanabashi *et al.* (Particle Data Group), Phys. Rev. D **98**, 030001 (2018).

39. E. Eichten, K. Gottfried, T. Kinoshita, K. Kogut, K. Lane, T. -M. Yan, Phys. Rev. Lett. **34**, 369 (1975), [Erratum: Phys. Rev. Lett. **36**, 1276 (1976)].
40. N. Isgur, Phys. Rev. D **60**, 054013 (1999).
41. R. A. Bertlmann, A. Martin, Nucl. Phys. B **168**, 111 (1980).
42. S. Nussinov, M. A. Lampert, Phys. Rep. **362**, 193 (2002).
43. J. D. Weinstein, N. Isgur, Phys. Rev. D **41**, 2236 (1990).
44. E. Braaten, M. Lu, Phys. Rev. D **77**, 014029 (2008).
45. T. Fernández-Caramés, A. Valcarce, J. Vijande, Phys. Rev. Lett. **103**, 222001 (2009).
46. J. -M. Richard, A. Valcarce, J. Vijande, Phys. Rev. D **95**, 054019 (2017).
47. H. Garcilazo, J. Phys. G **13**, L63 (1987).
48. P. del Amo Sánchez *et al.* (BaBar Collaboration), Phys. Rev. D **82**, 011101(R) (2010).
49. N. A. Törnqvist, Phys. Rev. Lett. **67**, 556 (1991).
50. Z. -F. Sun, J. He, X. Liu, Z. -G. Luo, S. -L. Zhu, Phys. Rev. D **84**, 054002 (2011).
51. J. Nieves, M. Pavón Valderrama, Phys. Rev. D **84**, 056015 (2011).
52. M. V. Polyakov, P. Schweitzer, Phys. Rev. D **98**, 034030 (2018).
53. T. Sugiura, Y. Ikeda, N. Ishii (HAL QCD Collaboration), EPJ Web Conf. **175**, 05011 (2018).
54. J. Vijande, A. Valcarce, N. Barnea, Phys. Rev. D **79**, 074010 (2009).
55. A. Francis, R. J. Hudspith, R. Lewis, K. Maltman, Phys. Rev. Lett. **118**, 142001 (2017).
56. M. Karliner, J. L. Rosner, Phys. Rev. Lett. **119**, 202001 (2017).
57. P. Bicudo, K. Cichy, A. Peters, M. Wagner, Phys. Rev. D **93**, 034501 (2016).
58. S. -Q. Luo, K. Chen, X. Liu, Y. -R. Liu, S. -L. Zhu, Eur. Phys. J. C **77**, 709 (2017).
59. M. -L. Du, W. Chen, X. -L. Chen, S. -L. Zhu, Phys. Rev. D **87**, 014003 (2013).
60. A. Czarnecki, B. Leng, M. B. Voloshin, Phys. Lett. B **778**, 233 (2018).
61. P. Jannnarkar, N. Mathur, M. Padmanath, Phys. Rev. D **99**, 034507 (2019).
62. L. Ma, Q. Wang, U. -G. Meissner, Phys. Rev. D **100**, 014028 (2019).
63. L. D. Faddeev, Sov. Phys. JETP **12**, 1014 (1961).
64. L. D. Faddeev, *Mathematical Aspects of the Three-Body Problem in Quantum Scattering Theory*, (Daley, New York, 1965).
65. J. Vijande, A. Valcarce, J. -M. Richard, Phys. Rev. D **76**, 114013 (2007).
66. E. Hernández, J. Nieves, J. M. Verde-Velasco, Phys. Rev. D **74**, 074008 (2006).
67. S. S. Agaev, K. Azizi, B. Barsbay, H. Sundu, Phys. Rev. D **99**, 033002 (2019).
68. T. Gershon, A. Poluektov, JHEP **1901**, 019 (2019).
69. G. Breit, E. Wigner, Phys. Rev. **49**, 519 (1936).
70. S. Ceci, A. Švarc, B. Zauner, D. M. Manley, S. Capstick, Phys. Lett. B **659**, 228 (2008).
71. S. Ceci, M. Korolija, B. Zauner, Phys. Rev. Lett. **111**, 112004 (2013).
72. D. V. Bugg, Int. J. Mod. Phys. A **24**, 394 (2009).
73. E. Braaten, M. Kusunoki, Phys. Rev. D **69**, 074005 (2004).
74. A. Pilloni, Act. Phys. Pol. B Proc. Supp. **7**, 463 (2014).